Single-Junction Polymer Solar Cells with Over 10% Efficiency by a Novel Two-Dimensional Donor–Acceptor Conjugated Copolymer

ARTICLE *in* ACS APPLIED MATERIALS & INTERFACES · FEBRUARY 2015

Impact Factor: 6.72 · DOI: 10.1021/am509047g · Source: PubMed

ACS APPLIED MATERIALS & INTERFACES

Research Article

www.acsami.org

Single-Junction Polymer Solar Cells with Over 10% Efficiency by a Novel Two-Dimensional Donor–Acceptor Conjugated Copolymer

Chang Liu,[†] Chao Yi,[†] Kai Wang,[†] Yali Yang,[‡] Ram S. Bhatta,[†] Mesfin Tsige,[†] Shuyong Xiao,*[,‡] and Xiong Gong*[,†]

[†]College of Polymer Science and Polymer Engineering, University of Akron, Akron, Ohio 44325, United States

[‡]1-Material Inc., 2290 Chemin St-Francois, Dorval, Quebec H9P 1K2, Canada

ABSTRACT: Recent advances in bulk heterojunction (BHJ) polymer solar cell (PSC) performance have resulted from compressing the band gap to enhance the short-circuit current density (J_{SC}) while lowering the highest occupied molecular orbital to increase the open-circuit voltage (V_{OC}) and consequently enhance the power conversion efficiencies (PCEs). However, PCEs of PSCs are still constrained by a low J_{SC}, small V_{OC}, and low fill factor (FF). In this study, we report 10.12% PCE from single-junction PSCs based on a novel two-dimensional (2D) conjugated copolymer. By introduction of conjugated 5-alkylthiophene-2-yl side chains to substitute nonconjugated alkoxy side chains in one-dimensional (1D) poly[[4,8-bis[(2-ethylhexyl)oxy]benzo[1,2-*b*:4,5-*b*′]dithiophene-2,6-diyl][3-fluoro-2-[(2-ethylhexyl)carbonyl]thieno[3,4-*b*]thiophenediyl]] (PTB7), a novel 2D donor–acceptor low-band-gap conjugated copolymer, poly[[4,8-bis[(5-ethylhexyl)thienyl]benzo[1,2-*b*;3,3-*b*]dithiophene-2,6-diyl][3-fluoro-2-[(2-ethylhexyl)carbonyl]thieno[3,4-*b*]thiophenediyl]] (PTB7-DT), is developed. 2D PTB7-DT is further systematically investigated by absorption spectroscopy, cyclic voltammetry, charge carrier mobility measurement, thin film morphology, and wide-angle X-ray diffraction and compared with 1D PTB7. In comparison with 1D PTB7, 2D PTB7-DT possesses a narrower band gap, tighter $\pi-\pi$ stacking, and higher charge carrier mobility. These results are consistent with the observation from first-principle calculations. Consequently, the single-junction PSCs based on 2D PTB7-DT exhibit a PCE of 10.12% with a high J_{SC}, larger V_{OC}, and high FF in comparison with the PSCs based on 1D PTB7.

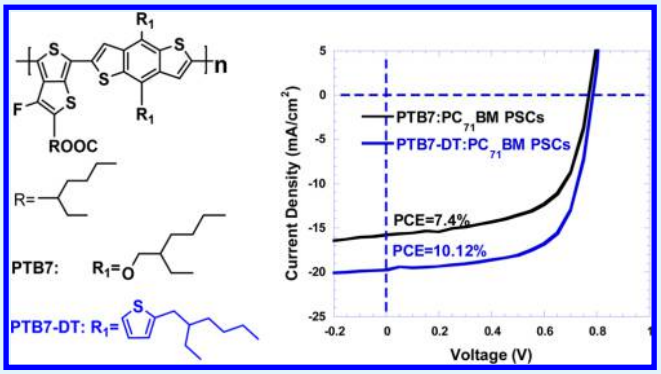

KEYWORDS: *single-junction polymer solar cells, 10 percent efficiency, two-dimensional conjugated polymer, PTB7 derivative, extended conjugation, compact $\pi-\pi$ stacking*

1. INTRODUCTION

In recent years, bulk heterojunction (BHJ) polymer solar cells (PSCs) have received great attention from both academic and industrial sectors as they are flexible and have large-scale production potential and low-cost grid power generation.[1,2] However, PSCs are still inferior to their inorganic counterparts in efficiency and stability.[3] To realize high-efficiency PSCs, significant work on the design of device structures and development of conjugated polymers with extended spectral coverage for wider solar absorption have been reported.[4−6] It has been proven that utilization of donor–acceptor (D–A) structures is an efficient strategy to obtain low-band-gap copolymers with modulated photoelectronic properties.[7−10] PSCs based on D–A copolymers have demonstrated the potential for high efficiency. Among these D–A low-band-gap conjugated copolymers, one-dimensional (1D) poly[[4,8-bis-[(2-ethylhexyl)oxy]benzo[1,2-*b*:4,5-*b*′]dithiophene-2,6-diyl][3-fluoro-2-[(2-ethylhexyl)carbonyl]thieno[3,4-*b*]thiophenediyl]] (PTB7) stands out as one of the most efficient conjugated polymer systems in production today.[11] However, the band gap of PTB7 is 1.68 eV, which is larger than the ideal band gap of the electron donor polymers for PSCs.[12] Moreover, the integrated photon flux using a band gap of 1.68 eV is ∼58%, which is much less than that of Si.[13] In addition, the hole mobility of PTB7 is smaller than that of fullerene derivatives,[14,15] which creates an unbalanced charge carrier transport in the BHJ composite, resulting in a low short-circuit current (J_{SC}) and low fill factor (FF) for BHJ PSCs.[16]

Two-dimensional (2D) conjugated polymers exhibit very interesting properties and promising photovoltaic performance as they possess two main absorption peaks: associated with conjugated main and side chains.[17−19] Moreover, they have a larger conjugated plane and higher interchain $\pi-\pi$ overlap than their 1D conjugated counterparts.[18] As a result, a broad and strong absorption band and high charge carrier mobility can be realized in 2D conjugated polymers.[18−20] Recently, Liao et al. reported over 10% efficiency from an inverted PSC fabricated by a BHJ active layer composed of 2D conjugated polymers as

Received: December 22, 2014
Accepted: February 11, 2015
Published: February 11, 2015

DOI: 10.1021/am509047g
ACS Appl. Mater. Interfaces 2015, 7, 4928−4935

Scheme 1. (a) Synthetic Routes for PTB7-DT and (b) Molecular Structure of PTB7

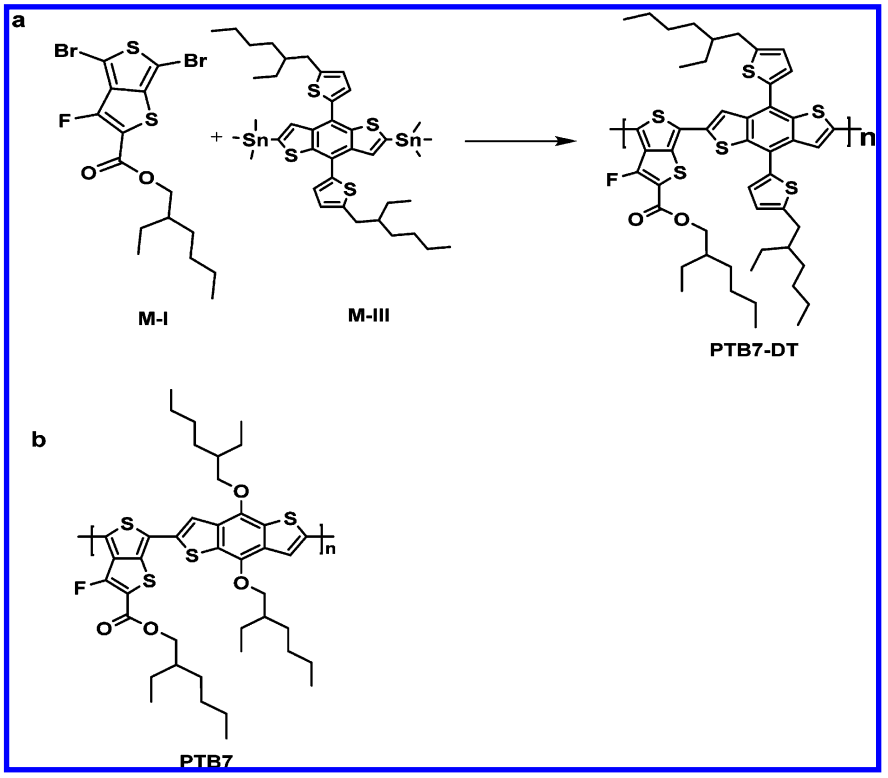

the electron donor and [6,6]-phenyl C71 butyric acid methyl ester ($PC_{71}BM$) as the electron acceptor and utilizing fullerene derivative doped ZnO as the electron extraction layer.[21,22] However, their work was mainly focused on the interface engineering, which has been previously reported.[23−26] To boost the efficiency of single-junction PSCs, herein, we report a novel 2D D−A low-band-gap conjugated copolymer. By substitution of nonconjugated alkoxy side chains (in 1D PTB7) with conjugated 5-alkylthiophene-2-yl side chains, 2D poly[[4,8-bis[(5-ethylhexyl)thienyl]benzo[1,2-*b*;3,3-*b*]dithiophene-2,6-diyl][3-fluoro-2-[(2-ethylhexyl)carbonyl]thieno[3,4-*b*]-thiophenediyl]] (PTB7-DT) is developed.[27−29] The two electron-rich conjugated 5-alkylthiophene-2-yl side chains make the electron-donating property of benzo[1,2-*b*:4,5-*b*′]dithiophene (BDT) stronger compared with that of the nonconjugated alkoxy side chains, resulting in an extended absorption coverage in PTB7-DT.[28] Moreover, the extended conjugation in thiophene units in 2D PTB7-DT facilitates the intermolecular $\pi-\pi$ interaction, which benefits the charge carrier mobility and absorption extension as well.[30,31] In addition, the introduction of two conjugated 5-alkylthiophene-2-yl side chains would lower the highest occupied molecular orbital (HOMO) energy level of PTB7-DT, resulting in an enlarged open-circuit voltage (V_{OC}) in PTB7-DT-based PSCs.[27] Consequently, 2D PTB7-DT-based PSCs exhibit a high J_{SC}, large V_{OC}, and high FF, with 10.12% efficiency from single-junction PSCs.

2. EXPERIMENTAL SECTION

2.1. Synthesis of PTB7-DT. PTB7-DT was synthesized through Stille coupling polymerization of a thieno[3,4-*b*]thiophenediyl derivative and 5-alkylthiophene-2-yl-substituted benzo[1,2-*b*:4,5-*b*′]-dithiophene derivative.[26] The detailed synthetic routes are described in Scheme 1a. The molecular structure of PTB7 is also shown in Scheme 1b for comparison.

2.2. UV−Vis Absorption Spectra and Cyclic Voltammetry Measurement. The thin films of PTB7 and PTB7-DT were cast from 1,2-dichlorobenzene (*o*-DCB) solutions onto quartz glass. UV−vis absorption spectra of these thin films were measured using an HP 8453 spectrophotometer.

Cyclic voltammetry (CV) measurements were carried out on a BAS C3-voltammetry cell stand equipped with a graphite electrode as the working electrode, a Ag/Ag^+ electrode as the reference electrode, and a Pt sheet as the counter electrode. The measurements were performed in the supporting electrolyte consisting of anhydrous acetonitrile (CH_3CN) mixed with tetrabutylammonium hexafluorophosphate ($((C4H_9)_4N(PF_6))$) under an argon atmosphere with a scan rate of 100 mV/s.

2.3. First-Principle Calculations. Ground-state density functional theory (DFT)[32] and time-dependent density functional theory (TDDFT)[33] calculations were performed using Becke's three-parameter Lee−Yang−Parr exchange-correlation functional (B3LYP)[34] with NWChem 6.1.[35] The dispersion correction was implemented using the Grimme approach.[36] All DFT and TDDFT calculations were performed at the NSF Teragrid supercomputer facility (Kraken at Oak Ridge National Laboratory).

Ground-state geometries of PTB7 and PTB7-DT oligomers were optimized at the B3LYP-D/3-21G* level, which has been proven to produce accurate conformational and electronic properties.[37,38] We assume a planar backbone, as might be imposed by the delocalization of p-electrons and crystal packing in the films. To obtain the energies of the frontier molecular orbitals, single-point calculations were performed at the B3LYP-D/6-31G* level starting from the optimized geometry. From ground-state calculations, the HOMO−LUMO (lowest unoccupied molecular orbital) gap was estimated from the HOMO and LUMO energies. TDDFT calculations of the vertical excitation energies of each PTB7 and PTB7-DT oligomer were performed at B3LYP/6-31G* starting from optimized geometries.

2.4. Thin Film Characterization. Tapping-mode atomic force microscopy (AFM) images were obtained by using a NanoScope NS3A system (Digital Instruments) to observe the surface morphologies of PTB7:$PC_{71}BM$ and PTB7-DT:$PC_{71}BM$ thin films. Transmission electron microscopy (TEM) experiments were carried

DOI: 10.1021/am509047g
ACS Appl. Mater. Interfaces 2015, 7, 4928−4935

out with a JEOL transmission electron microscope using an accelerating voltage of 120 kV. Wide-angle X-ray diffraction performed on a GE X-ray model XRD-6 was used to characterize the crystal orderings of PTB7-DT.

2.5. Mobility Measurement. The space charge limited current (SCLC) method was used to estimate the hole mobility of PTB7-DT and PTB7 thin films.[39,40] The mobility was determined by fitting the dark current observed from the hole-only diode according to the model of a single-carrier SCLC. The structure of the hole-only diode is ITO/PEDOT:PSS/PTB7-DT/MoO_3/Ag/Al, where ITO is indium tin oxide, PEDOT:PSS is poly(2,3-dihydrothieno-1,4-dioxin)−poly(styrenesulfonate), Ag is silver, and Al is aluminum, respectively. An approximately 230 nm thickness of PTB7-DT thin film was cast from an *o*-DCB solution. About 10 nm of MoO_3 and 5 nm of Ag (coated with 100 nm of Al) were sequentially deposited on top of the PTB7-DT layer in a vacuum system.

2.6. PSC Fabrication and Characterization. The PSC devices were fabricated using the conventional structure of ITO/PEDOT:PSS/PTB7-DT:$PC_{71}BM$/Al. The fabrication steps are as follows: Patterned ITO substrates were sequentially cleaned in an ultrasonic bath of detergent, deionized water, acetone, and 2-propanol. Subsequently, ITO substrates were dried in an oven overnight before treatment by UV-ozone for 20 min. A ∼40 nm layer of PEDOT:PSS was cast on top of the ITO substrates. Then the PTB7-DT:$PC_{71}BM$ BHJ composite was spin-coated onto ITO/PEDOT:PSS from an *o*-DCB solution mixed with 3% (by volume) 1,8-diiodoctane (DIO). The device fabrication was completed by thermal evaporation of 100 nm of Al as the cathode under vacuum at a base pressure of 2×10^{-6} Pa. The device area was 0.045 cm^2.

PSCs were measured under an AM1.5G calibrated solar simulator (Newport model 91160-1000). The light intensity was 100 mW/cm^2, which was calibrated by utilizing a monosilicon detector (with a KG-5 visible color filter) of the National Renewable Energy Laboratory (NREL) to reduce spectral mismatch. The current density−voltage (*J*−*V*) characteristics were recorded using a Keithley 2400 source meter.

3. RESULTS AND DISCUSSION

3.1. Synthesis and Characterization of PTB7-DT. Scheme 1 presents the synthetic routes for PTB7-DT. The details are as follows: A 1.03 g (2.18 mmol) mass of M-I (commercially available from 1-Material Inc., Canada), 1.97 g (2.18 mmol) of M-III (commercially available from 1-Material Inc.), 40 mL of toluene, and 40 mL of *N*,*N*-dimethylformamide (DMF) were charged into a 500 mL flask in an argon atmosphere to give a uniform solution. The obtained solution was bubbled with argon for 30 min and then mixed with 50 mg of tetrakis(triphenylphosphine)palladium. The mixed solution was stirred at 100 °C for 48 h. After 1 mL of phenyl bromide was added to the above solution, the resultant solution was further stirred for 5 h and then cooled to room temperature. Afterward, the mixture was poured into 2000 mL of methanol. The precipitated polymer was collected by filtration. The collected polymer was subjected to Soxhlet extraction in a sequence of acetone, hexane, and chloroform. The chloroform extraction was concentrated and then poured into acetone to cause the polymer to precipitate. The precipitated polymer was collected again by filtration and dried under vacuum overnight. A 1.77 g mass of purified polymer with a purple-black shine was yielded.

Figure 1 shows the ^1H NMR ($CDCl_3$) spectrum of PTB7-DT: δ −0.97 to +1.72 (br), 2.90 (br), 4.25 (br), 6.85−7.40 (br). GPC (elute in $CHCl_3$, polystyrene as standard): number-average molecular mass (M_n) of 45 000 Da and weight-average molecular mass (M_w) of 108 000 Da with a polydispersity (PD) of 2.4. The relatively low PD value for the electron donor polymer is favorable for approaching high-efficiency PSCs.[41]

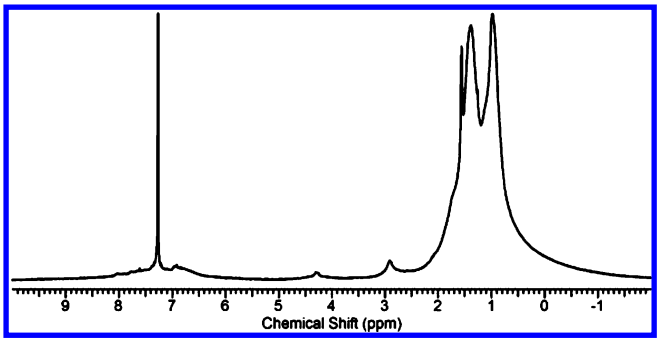

Figure 1. ^1H NMR ($CDCl_3$) spectrum of PTB7-DT.

3.2. Absorption Spectra of PTB7 and PTB7-DT Thin Films. Since PTB7 and PTB7-DT have similar molecular structures (Scheme 1), the comparison between them will provide useful information on the study of the influence of 2D conjugated structures on the photophysical and photovoltaic properties of D−A polymers. The UV−vis absorption spectra of PTB7-DT and PTB7 thin films are shown in Figure 2. The thin film of PTB7-DT shows a broadened absorption from 350 to 800 nm with a maximum peak at 704 nm, which coincides with the corresponding maximum photon flux region in the solar spectra (∼700 nm).[30] In comparison with PTB7, PTB7-DT exhibits an obvious red-shifted absorption spectrum which is likely attributed to the enhanced planarity of the new polymer chains by two conjugated 5-alkylthiophene-2-yl side chains.[42] Moreover, by incorporation of two conjugated 5-alkylthiophene-2-yl units in the side chain of BDT, PTB7-DT possesses two absorption peaks located at 325 and 708 nm. The first peak at 325 nm originates from the interaction between 5-alkylthiophene-2-yl side chains and the BDT unit along the vertical direction; the second peak at 708 nm originates from the intramolecular charge transfer absorption band.[43] The optical band gap of PTB7-DT (estimated from the onset of the thin film absorption) is decreased to 1.59 eV from 1.68 eV for PTB7. The 1.59 eV band gap is closer to the ideal band gap of donor polymers for PSCs.[12] In addition, two 5-alkylthiophene-2-yl units in the side chain of BDT could offer extended conjugation for conjugated polymers with 2D structure, which

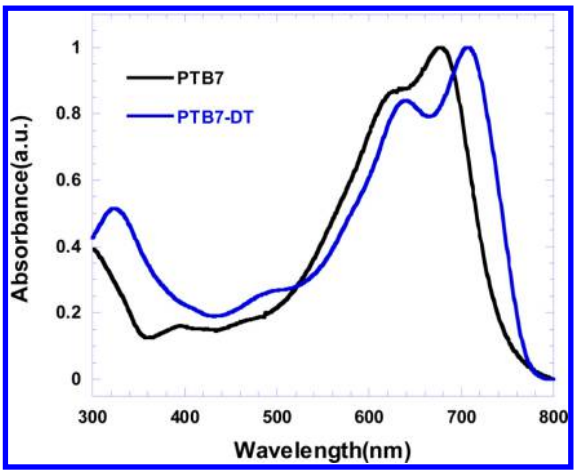

Figure 2. Absorption spectra of PTB7-DT and PTB7 thin films.

DOI: 10.1021/am509047g
ACS Appl. Mater. Interfaces 2015, 7, 4928−4935

facilitates intermolecular $\pi-\pi$ interaction, resulting in enhanced hole mobility of polymers (Figure 8).[27]

3.3. HOMO and LUMO Energy Levels of PTB7 and PTB7-DT. Enhanced conjugation in PTB7-DT can be visualized in terms of HOMO and LUMO energy level images. Figure 3 illustrates the well-delocalized HOMO and LUMO for

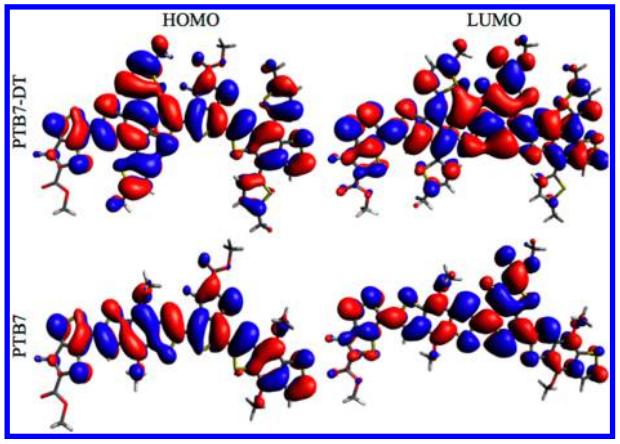

Figure 3. Images of the HOMO and LUMO orbitals for PTB7 and PTB7-DT dimers. Red and blue colors represent the negative and positive phases of the orbitals, respectively.

repeat units of both PTB7 and PTB7-DT. As is evident from Figure 3, the HOMO and LUMO wave functions in PTB7 are distributed along the backbone direction, which is 1D. Importantly, the presence of two 5-alkylthiophene-2-yl units in the BDT of PTB7-DT allows the HOMO and LUMO wave functions to be distributed in two dimensions. As a result, the electronic delocalization per monomer is increased by ~40% in PTB7-DT compared to PTB7. The presence of the 5-alkylthiophene-2-yl unit slightly lowered the HOMO level, lowered the LUMO level, and stabilized delocalization of electrons in a large area.

Parts a and b of Figure 4 present the CV curves of PTB7-DT and PTB7. The HOMO and LUMO energy levels are estimated from CV measurements following the equations $E_{HOMO} = -(E_{ox} + 4.8\ eV)$ and $E_{LUMO} = -(E_{red} + 4.8\ eV)$, where E_{ox} is 0.69 and 0.35 eV for PBT7-DT and PTB7 and E_{red} is −1.06 and −1.49 eV for PTB7-DT and PTB7, respectively. The HOMO energy levels of PTB7-DT and PTB7 are −5.49 and −5.15 eV, respectively. The LUMO energy levels of PTB7-DT and PTB7 are −3.74 and −3.31 eV, respectively. The HOMO and LUMO energy levels of PTB7 are consistent with the reported values.[11] Interestingly, it was found that both the LUMO and HOMO energy levels of PTB7-DT are simultaneously lowered by substitution of nonconjugated alkoxy side chains (in 1D PTB7) with conjugated 5-alkylthiophene-2-yl side chains (in 2D PTB7-DT), resulting in a narrower band gap of PTB7-DT with respect to that of 1D PTB7.[11] Figure 4c displays the HOMO and LUMO energy levels of PTB7-DT, PTB7, and $PC_{71}BM$, work functions of ITO, PEDOT:PSS, and Al. Since V_{OC} is proportional to the energy offset (ΔE, Figure 4c) between the HOMO energy level of donor polymers (PTB7-DT and PTB7) and the LUMO energy level of $PC_{71}BM$,[44] the lower lying HOMO energy level of PTB7-DT predicts a larger V_{OC} in PSCs made with PTB7-DT:$PC_{71}BM$ compared to PTB7:$PC_{71}BM$.

3.4. First-Principle Calculations. The observed energy gaps of PTB7 and PTB7-DT are supported by first-principle

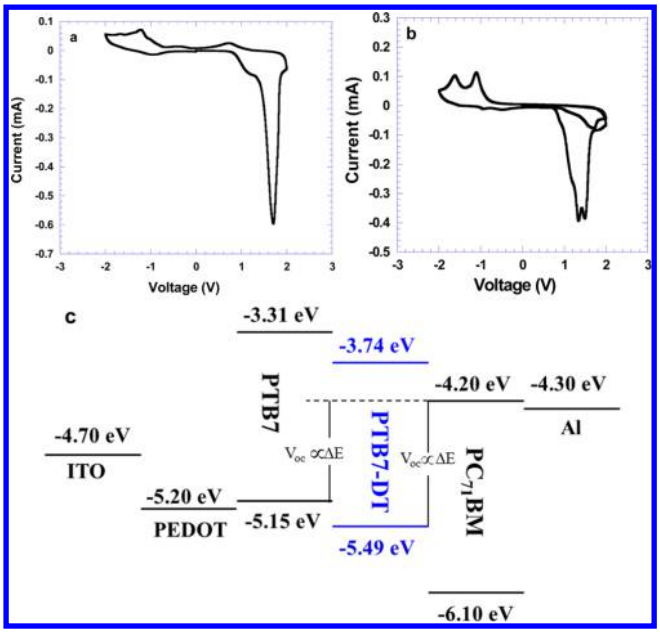

Figure 4. Cyclic voltammetry curves of (a) PTB7-DT and (b) PTB7 and (c) HOMO and LUMO energy levels of PTB7-DT, PTB7, and $PC_{71}BM$, work functions of ITO, PEDOT:PSS, and Al.

calculations shown in Figure 5. Both the HOMO−LUMO gap and optical gaps were extrapolated to the polymer limit using

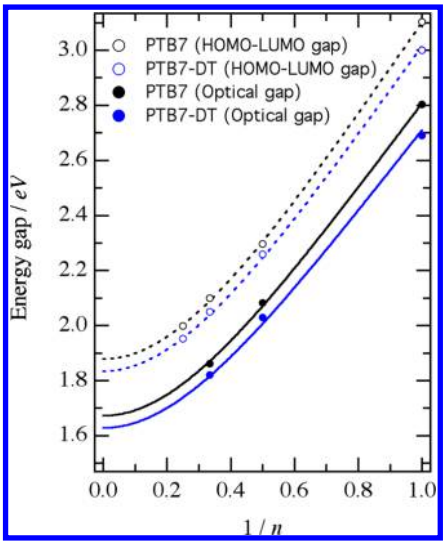

Figure 5. Energy gap as a function of the reciprocal of the number of monomer units ($1/n$) for PTB7 and PTB7-DT oligomers. Solid and dotted lines represent the extrapolation to the long-chain limit.

the Kuhn extrapolation technique, $E = E_0[1 + 2(k^n/k_0)\cos(\pi/N + 1)]^{1/2}$,[35] where $E_0 = (k_0/4\pi^2\mu_0)^{1/2}$ is the frequency of an isolated oscillator with $k^n/k_0 \approx -0.46$. N is the number of double bonds along the shortest backbone distance. The computed vertical excitation energies (optical band gaps) from the ground state (S_0) to the first excited state (S_1) of PTB7-DT oligomers are consistently lower compared to those of PTB7 oligomers. This trend is directly correlated to the ground-state HOMO−LUMO gaps because HOMO−LUMO gaps are higher than optical band gaps by the electrostatic binding energies of holes in S_0 and electrons in S_1. The computed optical band gap of PTB7 is higher than that of PTB7-DT,

DOI: 10.1021/am509047g
ACS Appl. Mater. Interfaces 2015, 7, 4928−4935

indicating that the introduction of the 5-alkylthiophene-2-yl side chain red shifts the optical band gap by ~0.07 eV. Similarly, the computed HOMO−LUMO gap of PTB7-DT is red-shifted by ~0.06 eV compared to the HOMO−LUMO gap of PTB7. These computed values of red shifts confirm the role of conjugated 5-alkylthiophene-2-yl side chains in lowerin the optical band gap and HOMO−LUMO gap as observed experimentally.

3.5. Crystal Ordering of PTB7 and PTB7-DT. Figure 6 shows AFM images of PTB7:$PC_{71}BM$ and PTB7-DT:$PC_{71}BM$

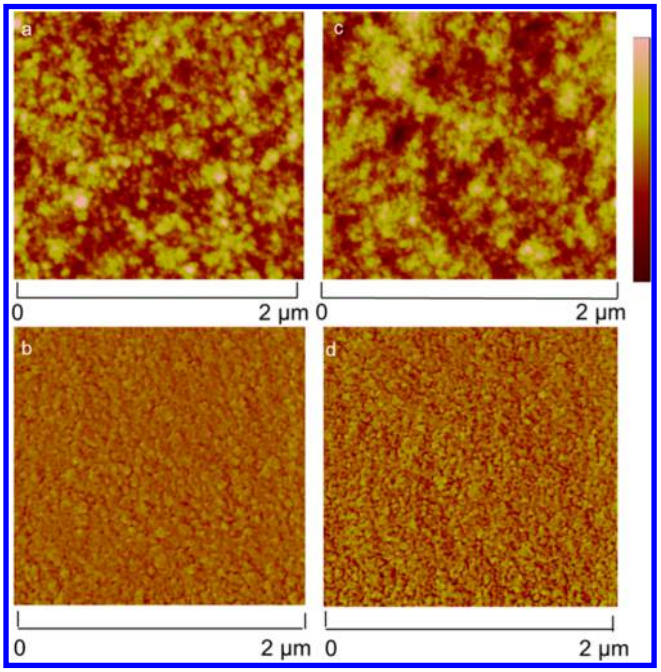

Figure 6. Atomic force microscopy images of PTB7:$PC_{71}BM$ (a, height image; b, phase image) and PTB7-DT:$PC_{71}BM$ (c, height image; d, phase image).

thin films. The thin film morphology of the BHJ active layer was significantly influenced by the incorporation of 5-alkylthiophene-2-yl side chains into PTB7. The PTB7-DT:$PC_{71}BM$ BHJ thin film exhibits a relatively larger root mean squared (RMS) roughness of 3.2 nm than that of PTB7:$PC_{71}BM$ (1.7 nm), suggesting a better ordering of PTB7-DT chains in the BHJ film and thus a high crystallinity of the BHJ composite.[45] To confirm these assumptions, wide-angle X-ray diffraction (WAXD) was carried out to inspect the macromolecular accumulation.[46] The WAXD patterns of PTB7-DT and PTB7 thin films are shown in Figure 7. The peak at 21° reveals a short $\pi-\pi$ distance of 3.5 Å for PTB7-DT, which is smaller than the $\pi-\pi$ distance of PTB7 (3.8 Å).[44] The shorter $\pi-\pi$ distance of PTB7-DT indicates that polymer main chains are more likely to form a planar conformation in a solid film, resulting in a red-shifted absorption spectrum, which is in good agreement with the absorption of PTB7-DT (Figure 2). The planarity of the main chain and the short $\pi-\pi$ distance would facilitate charge transport, resulting in high hole mobility for PTB7-DT.[47]

3.6. Hole Mobilities of PTB7 and PTB7-DT. Hole mobility is estimated by the SCLC method based on current density−voltage ($J-V$) characterization from hole-only diodes. The $J-V$ characterizations of the hole-only diode with a structure of ITO/PEDOT:PSS/PTB7-DT (or PTB7)/MoO_3/

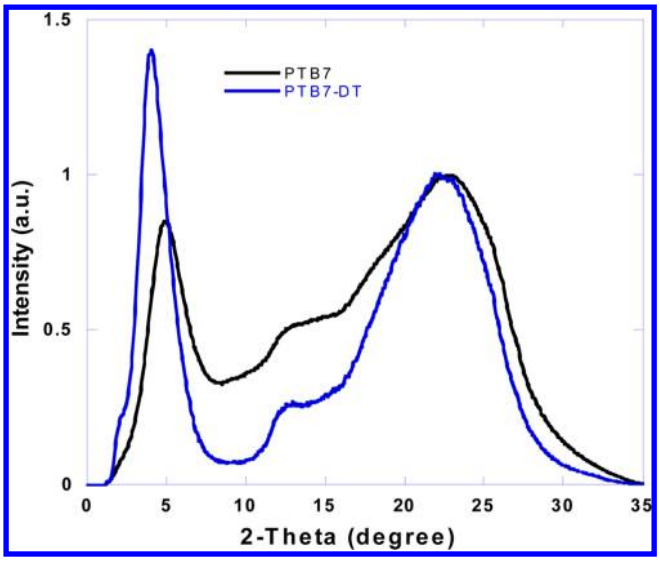

Figure 7. Wide-angle X-ray diffraction patterns of PTB7 and PTB7-DT thin films.

Ag are shown in Figure 8, where MoO_3 is molybdenum trioxide and Ag is silver. The hole mobilities are estimated to be 8.0 ×

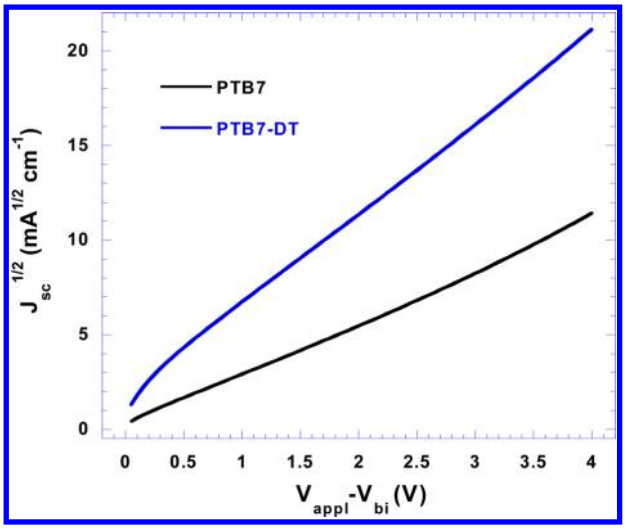

Figure 8. Current−voltage characteristics of a hole-only device with an architecture of ITO/PEDOT/PTB7 (or PTB7-DT)/MoO_3/Al.

10^{-4} $cm^2/(V\ s)$ for PTB7-DT and 1.9 × 10^{-4} $cm^2/(V\ s)$ for PTB7.[14] Thus, high PCEs are anticipated from PTB7-DT:$PC_{71}BM$-based PSCs.[48]

3.7. Film Morphologies of BHJ Composite Thin Films. Figure 9 presents TEM images of the phase separation in PTB7-DT:$PC_{71}BM$ and PTB7:$PC_{71}BM$ thin films. Obviously, larger domains are observed in PTB7:$PC_{71}BM$ thin films than in PTB7-DT:$PC_{71}BM$ thin films. These larger domains certainly hinder the exciton migration to the interfaces between PTB7 and $PC_{71}BM$, resulting in unfavorable charge separation. However, there is no large phase separation within PTB7-DT:$PC_{71}BM$ thin films, which suggests a much better miscibility formed between PTB7-DT and $PC_{71}BM$, resulting in a preferable interpenetrating network. As a result, an enhanced PCE is expected from PTB7-DT:$PC_{71}BM$-based PSCs.[49]

DOI: 10.1021/am509047g
ACS Appl. Mater. Interfaces 2015, 7, 4928−4935

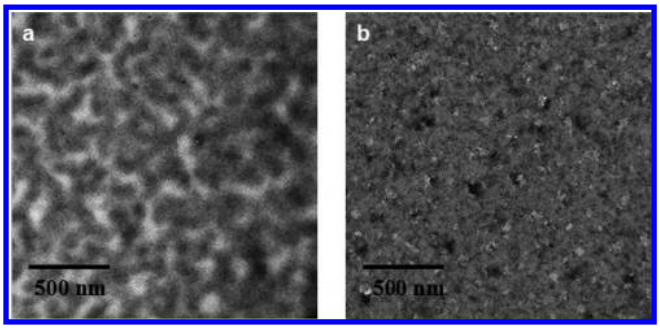

Figure 9. Transmission electronic microscopy images of (a) PTB7:$PC_{71}BM$ and (b) PTB7-DT:$PC_{71}BM$ thin films.

3.8. Device Performance of Single-Junction PSCs. The photovoltaic properties of PTB7-DT are studied in BHJ PSCs with a device structure of ITO/PEDOT:PSS/PTB7-DT:$PC_{71}BM$/Al. The PSC performance was first optimized by processing a PTB7-DT:$PC_{71}BM$ (1:1 by weight) BHJ thin film from an *o*-DCB solution mixed with 3% DIO. Similar to that of PSCs fabricated by the PTB7:$PC_{71}BM$ BHJ composite,[11] PSCs fabricated by PTB7-DT:$PC_{71}BM$ show dramatically increased J_{SC}, FF, and PCE. J_{SC} reaches 17.8 mA/cm^2 from 14.6 mA/cm^2, FF reaches 60% from 58%, and the corresponding PCE reaches 8.50% from 6.80% for the PSCs processed with an *o*-DCB solution with DIO as compared with those processed without DIO. The device performance of PSCs was optimized by tuning the weight ratio of PTB7-DT to $PC_{71}BM$. With a thickness of the BHJ active layer of ∼85 nm, the best PCEs were observed from PSCs fabricated by PTB7-DT:$PC_{71}BM$ with a 1:1.5 weight ratio. Under this condition, a J_{SC} of 18.7 mA/cm^2, a V_{OC} of 0.79 V, an FF of 64.0%, and a corresponding PCE of 9.50% were observed. To further boost the PCE of PSCs, the thicknesses of the BHJ composite active layer were optimized. Table 1 summarizes the device performance parameters. The PCEs dependent on the film thickness of the PTB7-DT:$PC_{71}BM$ BHJ composite are shown in Figure 10a. As shown in Figure 10a, the highest PCE is obtained from the PSCs with a BHJ film thickness of ca. 100 nm. As the BHJ film thicknesses are further increased, the PCEs are decreased. The *J*−*V* characterizations of PSCs based on PTB7-DT:$PC_{71}BM$ and PTB7-DT:$PC_{71}BM$ are shown in Figure 10b. The PSCs fabricated by PTB7:$PC_{71}BM$ with a thickness of 100 nm exhibit a J_{SC} of 15.8 mA/cm^2, a V_{OC} of 0.76 V, an FF of 62%, and a corresponding PCE of 7.40%. These device performance parameters are consistent with the reported values from Yu's group.[11] Under the same conditions, the PTB7-DT-based PSCs exhibit a J_{SC} of 19.78 mA/cm^2, a V_{OC} of 0.79 V, an FF of 65.0%, and a corresponding PCE of 10.12%. More than 60 devices are fabricated and characterized; the deviation in PCE is less than 6%. The PCEs from PTB7-DT:$PC_{71}BM$-based PSCs are enhanced more than 36% as compared to those from PTB7:$PC_{71}BM$-based PSCs.

The shunt (R_{SH}) and series (R_S) resistances are estimated from *J*−*V* curves as shown in Figure 10b. R_{SH} and R_S for PTB7-DT:$PC_{71}BM$-based PSCs are ∼1500 and ∼2 Ω cm^2, respectively. R_{SH} and R_S for PTB7:$PC_{71}BM$-based PSCs are ∼1000 and ∼10 Ω cm^2, respectively. The smaller R_S indicates that there is a favorable charge carrier transport within PSCs. On the other hand, the larger R_{SH} indicates that the reverse current densities are smaller, resulting in an enlarged FF. Thus, an enhanced PCE is anticipated from PSCs made with PTB7-DT:$PC_{71}BM$ rather than PTB7:$PC_{71}BM$.

Increased V_{OC} (0.79 V) for PTB7-DT:$PC_{71}BM$-based PSCs was observed, in comparison with that (0.76 V) of PTB7:$PC_{71}BM$-based PSCs. The origin of the enhancement is the introduction of 5-alkylthiophene-2-yl units into the BDT units, which leads to enhanced planarity of the polymer chains (as evidenced in Figure 3) and consequently gives rise to the lowered HOMO energy level of PTB7-DT. Since V_{OC} is proportional to the energy level offset between the HOMO energy level of the electron donor polymer and the LUMO energy level of the electron acceptor, the augmented energy offset between PTB7-DT and $PC_{71}BM$ leads to an enhanced V_{OC} observed from the PSC device. This observation is consistent with the band alignment shown in Figure 4c.

Figure 10c shows the external quantum efficiency (EQE) spectra of PTB7-DT:$PC_{71}BM$- and PTB7:$PC_{71}BM$-based PSCs. The PTB7-DT:$PC_{71}BM$-based PSCs exhibit a broad and high response range, covering from 350 to 800 nm, with a maximum EQE of 86% at 697 nm, while the PTB7:$PC_{71}BM$-based PSCs exhibit a relatively narrower and lower response, covering from 350 to 750 nm. Moreover, in the range from 350 to 400 nm, PTB7-DT:$PC_{71}BM$-based PSCs show a much higher EQE value than the PTB7:$PC_{71}BM$-based PSCs, which is in good agreement with the UV−vis absorption spectra of PTB7-DT and PTB7 shown in Figure 2. J_{SC} values estimated from the integration of the EQE spectra with an AM1.5G reference spectrum are 18.95 and 14.76 mA/cm^2 for PTB7-DT:$PC_{71}BM$-based PSCs and PTB7:$PC_{71}BM$-based PSCs, respectively. These values are consistent with those obtained from the *J*−*V* characteristics under a standard one-solar simulator (Figure 10b).

4. CONCLUSIONS

A novel 2D D−A low-band-gap conjugated copolymer, PTB7-DT, was developed for polymer photovoltaic application. Compared with 1D PTB7, 2D PTB7-DT shows a more pronounced red-shifted absorption spectrum, higher hole mobility, and deeper HOMO energy level. These observations

Table 1. Device Performance of PSCs[a]

	BHJ layer thickness (nm)	V_{OC} (V)	J_{SC} (mA/cm^2)	FF (%)	PCE (%)
1:1	∼85	0.79	17.8 (17.0 ± 0.9)	61 (59 ± 3)	8.57 (8.23 ± 0.4)
1:1.5	∼60	0.79	16.9 (16.9 ± 0.4)	62 (62 ± 2)	8.20 (8.20 ± 0.1)
	∼85	0.79	18.7 (18.3 ± 0.5)	64 (62 ± 3)	9.50 (9.30 ± 0.3)
	∼100	0.79	19.6 (19.6 ± 0.3)	65 (65 ± 1)	10.12 (10.12 ± 0.2)
	∼120	0.79	17.9 (17.9 ± 0.4)	63 (63 ± 2)	8.80 (8.80 ± 0.2)
	∼150	0.78	16.6 (16.6 ± 0.5)	62 (62 ± 3)	7.90 (7.90 ± 0.3)
1:2	∼85	0.79	18.3 (17.8 ± 0.6)	62 (60 ± 4)	8.92 (8.60 ± 0.4)

[a]Device average values are based on more than 60 devices. The average values and deviations are given in parentheses.

DOI: 10.1021/am509047g
ACS Appl. Mater. Interfaces 2015, 7, 4928−4935

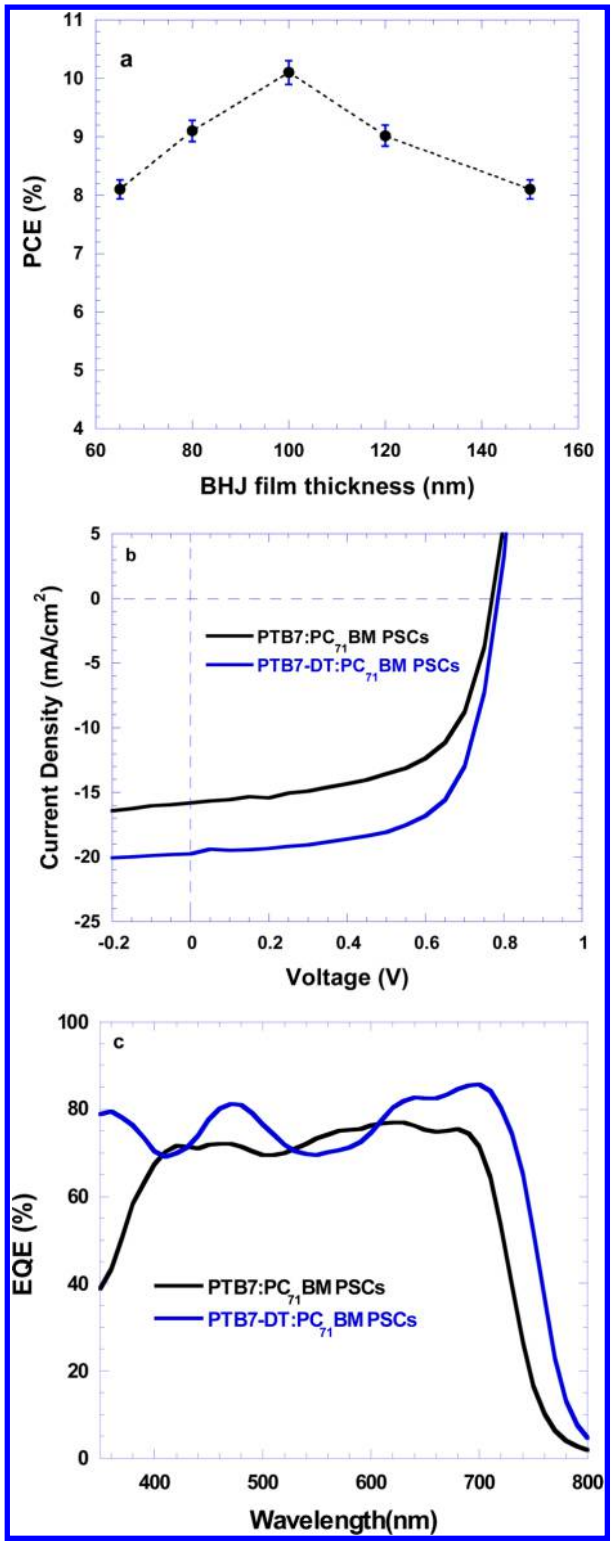

Figure 10. (a) PCEs of PSCs with different film thicknesses of the PTB7-DT:PC$_{71}$BM BHJ active layer. (b) *J*–*V* characterization of PTB7-DT:PC$_{71}$BM- and PTB7:PCBM-based PSCs under white light illumination. (c) External quantum efficiencies of PSCs fabricated by PTB7:PC$_{71}$BM and PTB7-DT:PC$_{71}$BM with a BHJ layer thickness of 100 nm.

are consistent with first-principle calculations. As a result, PTB7-DT exhibits efficiency over 10% from single-junction polymer solar cells.

AUTHOR INFORMATION

Corresponding Authors

*E-mail: steven.xiao@1-material.com.
*E-mail: xgong@uakron.edu.

Notes

The authors declare no competing financial interest.

ACKNOWLEDGMENTS

We at The University of Akron are thankful for National Science Foundation Grant 1351785.

REFERENCES

(1) Coakley, K. M.; McGehee, M. D. Conjugated Polymer Photovoltaic Cells. *Chem. Mater.* **2004**, *16*, 4533–4542.
(2) Brabec, C. J.; Sariciftci, N. S.; Hummelen, J. C. Plastic Solar Cells. *Adv. Funct. Mater.* **2001**, *11*, 15–26.
(3) Green, M. A.; Emery, K.; Hishikawa, Y.; Warta, W.; Dunlop, E. D. Solar Cell Efficiency Tables (Version 39). *Prog. Photovoltaics* **2012**, *20*, 12–20.
(4) Gong, X. Towards High Performance Inverted Polymer Solar Cells. *Polymer* **2012**, *53*, 5437–5448.
(5) Ameri, T.; Li, N.; Brabec, C. J. Highly Efficient Organic Tandem Solar Cells: A Follow Up Review. *Energy Environ. Sci.* **2013**, *6*, 2390–2413.
(6) Zhang, F.; Mammo, W.; Andersson, L. M.; Admassie, S.; Andersson, M. R.; Inganäs, O. Low-Bandgap Alternating Fluorene Copolymer/Methanofullerene Heterojunctions in Efficient Near-Infrared Polymer Solar Cells. *Adv. Mater.* **2006**, *18*, 2169–2173.
(7) Hou, J.; Chen, H.; Zhang, S.; Li, G.; Yang, Y. Synthesis, Characterization, and Photovoltaic Properties of a Low Band Gap Polymer Based on Silole-Containing Polythiophenes and 2,1,3-Benzothiadiazole. *J. Am. Chem. Soc.* **2008**, *130*, 16144–16145.
(8) Chu, T.; Lu, J.; Beaupr, S.; Zhang, Y.; Pouliot, J.; Wakim, S.; Zhou, J.; Leclerc, M.; Li, Z.; Ding, J.; Tao, Y. Bulk Heterojunction Solar Cells Using Thieno[3,4-*c*]pyrrole-4,6-dione and Dithieno[3,2-*b*:20,30-*d*]silole Copolymer with a Power Conversion Efficiency of 7.3%. *J. Am. Chem. Soc.* **2011**, *133*, 4250–4253.
(9) Zhang, M.; Fan, H.; Guo, X.; He, Y.; Zhang, Z.; Min, J.; Zhang, J.; Zhan, X.; Li, Y. Synthesis and Photovoltaic Properties of Bithiazole-Based Donor-Acceptor Copolymers. *Macromolecules* **2010**, *43*, 5706–5712.
(10) Zhang, M.; Guo, X.; Li, Y. Synthesis and Characterization of a Copolymer Based on Thiazolothiazole and Dithienosilole for Polymer Solar Cells. *Adv. Energy Mater.* **2011**, *1*, 557–560.
(11) Liang, Y.; Xu, Z.; Xia, J.; Tsai, S. T.; Wu, Y.; Li, G.; Ray, C.; Yu, L. For the Bright Future—Bulk Heterojunction Polymer Solar Cells with Power Conversion Efficiency of 7.4%. *Adv. Mater.* **2010**, *22*, E135–E138.
(12) Scharber, M. C.; Mühlbacher, D.; Koppe, M.; Denk, P.; Waldauf, C.; Heeger, A. J.; Brabec, C. J. Design Rules for Donors in Bulk-Heterojunction Solar Cells—Towards 10% Energy-Conversion Efficiency. *Adv. Mater.* **2006**, *18*, 789–794.
(13) Geist, J.; Gladden, W. K.; Zalewski, E. F. Physics of Photon-Flux Measurements with Silicon Photodiodes. *J. Opt. Soc. Am.* **1982**, *72*, 1068–1075.
(14) Wang, H.; Yu, X.; Yi, C.; Ren, H.; Liu, C.; Yang, Y.; Xiao, S.; Zheng, J.; Karim, A.; Cheng, S. Z. D.; Gong, X. Fine-Tuning of Fluorinated Thieno[3,4-*b*]thiophene Copolymer for Efficient Polymer Solar Cells. *J. Phys. Chem. C* **2013**, *117*, 4358–4363.
(15) Mihailetchi, V. D.; Wildeman, J.; Blom, P. W. M. Space-Charge Limited Photocurrent. *Phys. Rev. Lett.* **2005**, *94*, 126602.
(16) Kotlarski, J. D.; Blom, P. W. M. Impact of Unbalanced Charge Transport on the Efficiency of Normal and Inverted Solar Cells. *Appl. Phys. Lett.* **2012**, *100*, 013306.
(17) Hou, J.; Tan, Z.; Yan, Y.; He, Y.; Yang, C.; Li, Y. Synthesis and Photovoltaic Properties of Two-Dimensional Conjugated Polythio-

DOI: 10.1021/am509047g
ACS Appl. Mater. Interfaces 2015, 7, 4928–4935

phenes with Bi(thienylenevinylene) Side Chains. *J. Am. Chem. Soc.* **2006**, *14*, 4911−4916.
(18) Hou, J.; Huo, L.; He, C.; Yang, C.; Li, Y. Synthesis and Absorption Spectra of Poly(3-(phenylenevinyl)thiophene)s with Conjugated Side Chains. *Macromolecules* **2006**, *39*, 594−603.
(19) Hou, J.; Tan, Z.; He, Y.; Yang, C.; Li, Y. Branched Poly(thienylene vinylene)s with Absorption Spectra Covering the Whole Visible Region. *Macromolecules* **2006**, *39*, 4657−4662.
(20) Liu, P.; Zhang, K.; Liu, F.; Jin, Y.; Liu, S.; Russell, P. T.; Yip, H.-L.; Huang, F.; Cao, Y. Effect of Fluorine Content in Thienothiophene-Benzodithiophene Copolymers on the Morphology and Performance of Polymer Solar Cells. *Chem. Mater.* **2014**, *26*, 3009−3017.
(21) Liao, S.-H.; Jhuo, H.-J.; Cheng, Y.-S.; Chen, S.-A. Fullerene Derivative-Doped Zinc Oxide Nanofilm as the Cathode of Inverted Polymer Solar Cells with Low-Bandgap Polymer (PTB7-Th) for High Performance. *Adv. Mater.* **2013**, *25*, 4766−4771.
(22) Liao, S.-H.; Jhuo, H.-J.; Yeh, P.-N.; Cheng, Y.-S.; Li, Y.-L.; Lee, Y.-H.; Sharma, S.; Chen, S.-A. Single Junction Inverted Polymer Solar Cell Reaching Power Conversion Efficiency 10.31% by Employing Dual-Doped Zinc Oxide Nano-Film as Cathode Interlayer. *Sci. Rep.* **2014**, DOI: 10.1038/srep06813.
(23) Yang, T.; Wang, M.; Duan, C.; Hu, X.; Huang, L.; Peng, J.; Huang, F.; Gong, X. Inverted Polymer Solar Cells with 8.4% Efficiency by Conjugated Polyelectrolyte. *Energy Environ. Sci.* **2012**, *5*, 8208−8214.
(24) Yi, C.; Yue, K.; Zhang, W.-B.; Lu, X.; Hou, J.; Li, Y.; Huang, L.; Newkome, G. R.; Cheng, S. Z. D.; Gong, X. Conductive Water/Alcohol-Soluble Neutral Fullerene Derivative as an Interfacial Layer for Inverted Polymer Solar Cells with High Efficiency. *ACS Appl. Mater. Interfaces* **2014**, *6*, 14189−14195.
(25) Zhang, K.; Zhong, C.; Liu, S.; Mu, C.; Li, Z.; Yan, H.; Huang, F.; Cao, Y. Highly Efficient Inverted Polymer Solar Cells Based on a Crosslinkable Water-/Alcohol-Soluble Conjugated Polymer Interlayer. *ACS Appl. Mater. Interfaces* **2014**, *6*, 10429−10435.
(26) He, Z.; Zhong, C.; Su, S.; Xu, M.; Wu, H.; Cao, Y. Enhanced Power-Conversion Efficiency in Polymer Solar Cells Using an Inverted Device Structure. *Nat. Photonics* **2012**, *6*, 591−595.
(27) Xiao, S. Y.; Yang, Y. L. Poly[[2,6′-4,8-di(5-ethylhexylthienyl)-benzo[1,2-b;3,3-b]dithiophene][3-fluoro-2[(2- ethylhexyl)carbonyl]-thieno[3,4-b]thiophenediyl]]. U.S. Patent 13/987,006, June 25, 2013.
(28) Chen, J.-D.; Cui, C.; Li, Y.-Q.; Zhou, L.; Ou, Q.-D.; Li, C.; Li, Y.; Tang, J.-X. Single-Junction Polymer Solar Cells Exceeding 10% Power Conversion Efficiency. *Adv. Mater.* **2015**, *27*, 1035−1041.
(29) Yin, Z.; Zheng, Q.; Chen, S.-C.; Li, J.; Cai, D.; Ma, Y.; Wei, J. Solution-Derived Poly(ethylene glycol)-TiO_x Nanocomposite Film as a Universal Cathode Buffer Layer for Enhancing Efficiency and Stability of Polymer Solar Cells. *Nano Res.* **2014**, DOI: 10.1007/s12274-014-0615-8.
(30) Hou, L.; Zhang, S.; Guo, X.; Xu, F.; Li, Y.; Hou, J. Replacing Alkoxy Groups with Alkylthienyl Groups: A Feasible Approach To Improve the Properties of Photovoltaic Polymers. *Angew. Chem., Int. Ed.* **2011**, *50*, 9697−9702.
(31) Pang, H.; Vilela, F.; Skabara, P. J.; McDouall, J. J. W.; Crouch, D. J.; Anthopoulos, T. D.; Bradley, D. D. C.; De Leeuw, D. M.; Horton, P. N.; Hursthouse, M. B. Advantageous 3D Ordering of p-Conjugated Systems: A New Approach towards Efficient Charge Transport in Any Direction. *Adv. Mater.* **2007**, *19*, 4438−4442.
(32) Hohenberg, P.; Kohn, W. Inhomogeneous Electron Gas. *Phys. Rev.* **1964**, *136*, B864−B871.
(33) Runge, E.; Gross, E. K. U. Density-Functional Theory for Time-Dependent Systems. *Phys. Rev. Lett.* **1984**, *52*, 997−1000.
(34) Becke, A. D. Density functional Thermochemistry. III. The Role of Exact Exchange. *J. Chem. Phys.* **1993**, *98*, 5648−5652.
(35) Valiev, M.; Bylaska, E. J.; Govind, N.; Kowalski, K.; Straatsma, T. P.; van Dam, H. J. J.; Wang, D.; Nieplocha, J.; Apra, E.; Windus, T. L.; de Jong, W. A. NWChem: A Comprehensive and Scalable Open-Source Solution for Large Scale Molecular Simulations. *Comput. Phys. Commun.* **2010**, *181*, 1477−1489.
(36) Grimme, S. Semiempirical GGA-Type Density Functional Constructed with a Long-Range Dispersion Correction. *J. Comput. Chem.* **2006**, *27*, 1787−1799.
(37) Bhatta, R. S.; Perry, D. S.; Tsige, M. Nanostructures and Electronic Properties of a High-Efficiency Electron-Donating Polymer. *J. Phys. Chem. A* **2013**, *117*, 12628−12634.
(38) Kuhn, W. Über das Absorptions Spectrum der Polyene. *Helv. Chim. Acta* **1948**, *31*, 1780−1799.
(39) Mihailetchi, V. D.; Koster, L. J. A.; Blom, P. W. M.; Melzer, C.; De Boer, B.; van Duren, J. K. J.; Janssen, R. A. J. Compositional Dependence of the Performance of Poly(*p*-phenylene vinylene): Methanofullerene Bulk Heterojunction Solar Cells. *Adv. Funct. Mater.* **2005**, *15*, 795−801.
(40) Campbell, I. H.; Hagler, T. W.; Smith, D. L. Direct Measurement of Conjugated Polymer Electronic Excitation Energies Using Metal/Polymer/Metal Structures. *Phys. Rev. Lett.* **1996**, *76*, 1900−1903.
(41) Olsen, B. D.; Jang, S. Y.; Lüning, J. M.; Segalman, R. A. Higher Order Liquid Crystalline Structure in Low-Polydispersity DEH-PPV. *Macromolecules* **2006**, *39*, 4469−4479.
(42) Li, Y. Molecular Design of Photovoltaic Materials for Polymer Solar Cells: Toward Suitable Electronic Energy Levels and Broad Absorption. *Acc. Chem. Res.* **2011**, *45*, 723−733.
(43) Beaujuge, P. M.; Amb, C. M.; Reynolds, J. R. Spectral Engineering in π-Conjugated Polymers with Intramolecular Donor−Acceptor Interactions. *Acc. Chem. Res.* **2010**, *43*, 1396−1407.
(44) Brabec, C. H.; Cravino, A.; Meissner, D.; Sariciftci, N. S.; Fromherz, T.; Rispens, M. T.; Sanchez, L.; Hummelen, J. C. Origin of the Open Circuit Voltage of Plastic Solar Cells. *Adv. Funct. Mater.* **2001**, *11*, 374−380.
(45) Li, G.; Shrotriya, V.; Huang, S.; Yao, Y.; Moriarty, T.; Emery, K.; Yang, Y. High-Efficiency Solution Processable Polymer Photovoltaic Cells by Self-Organization of Polymer Blends. *Nat. Mater.* **2005**, *4*, 864−868.
(46) Somani, R. H.; Hsiao, B. S.; Nogales, A. Structure Development during Shear Flow Induced Crystallization of i-PP: In Situ Wide-Angle X-ray Diffraction Study. *Macromolecules* **2001**, *34*, 5902−5909.
(47) Szarko, J. M.; Guo, J.; Rolczynski, B. S.; Chen, L. Current Trends in the Optimization of Low Band Gap Polymers in Bulk Heterojunction Photovoltaic Devices. *J. Mater. Chem.* **2011**, *21*, 7849−7857.
(48) Liu, C.; Wang, K.; Hu, X.; Yang, Y.; Hsu, C. H.; Zhang, W.; Xiao, S.; Gong, X.; Cao, Y. Molecular Weight Effect on the Efficiency of Polymer Solar Cells. *ACS Appl. Mater. Interfaces* **2013**, *5*, 12163−12167.
(49) Ma, W.; Yang, C.; Gong, X.; Lee, K.; Heeger, A. J. Thermally Stable, Efficient Polymer Solar Cells with Nanoscale Control of the Interpenetrating Network Morphology. *Adv. Funct. Mater.* **2005**, *15*, 1617−1622.

DOI: 10.1021/am509047g
ACS Appl. Mater. Interfaces 2015, 7, 4928−4935